Sequential Place Learning: Heuristic-Free High-Performance Long-Term Place Recognition

Marvin Chancán, Michael Milford

Abstract—Sequential matching using hand-crafted heuristics has been standard practice in route-based place recognition for enhancing pairwise similarity results for nearly a decade. However, precision-recall performance of these algorithms dramatically degrades when searching on short *temporal window* (TW) lengths, while demanding high compute and storage costs on large robotic datasets for autonomous navigation research. Here, influenced by biological systems that robustly navigate spacetime scales even without vision, we develop a *joint visual and positional representation learning* technique, via a *sequential process*, and design a learning-based CNN+LSTM architecture, trainable via backpropagation through time, for viewpoint- and appearance-invariant place recognition. Our approach, *Sequential Place Learning* (SPL), is based on a CNN function that visually encodes an environment from a single traversal, thus reducing storage capacity, while an LSTM temporally fuses each visual embedding with corresponding positional data—obtained from any source of motion estimation—for direct sequential inference. Contrary to classical two-stage pipelines, *e.g.*, *match-then-temporally-filter*, our network directly eliminates false-positive rates while jointly learning sequence matching from a single monocular image sequence, even using short TWs. Hence, we demonstrate that our model outperforms 15 classical methods while setting *new state-of-the-art* performance standards on 4 challenging benchmark datasets, where one of them can be considered solved with recall rates of 100% at 100% precision, correctly matching *all* places under extreme sunlight-darkness changes. In addition, we show that SPL can be up to 70× faster to deploy than classical methods on a 729 km route comprising 35,768 consecutive frames. Extensive experiments demonstrate the potential of this framework through quantitative and qualitative results. Baseline code available at https://github.com/mchancan/deepseqslam

Fig. 1. **Average Precision vs. Testing Latency**. For testing, we sampled 3K+ frames of the 729 km Nordland dataset for better visualization of deployment latencies. All our models achieve comparable results to the best SeqSLAM settings, even using short TW, while being $\sim 10\times$ faster to deploy. Our approach can be $\sim 60\times$ faster than classical methods on the full 35K+ frames. *Note:* Speed-up values are based on average latencies of our model running on CPU, as classical methods can be deployed on CPU only.

I. INTRODUCTION

The vast majority of sequential filtering algorithms in place recognition research for autonomous robot navigation are variants of carefully designed, complex hand-crafted heuristics. The use of these algorithms on top of pre-computed global image descriptors based on convolutional neural networks (CNN) [16] has enabled researchers to improve significantly accuracies on challenging driving datasets under viewpoint and appearance changes, *e.g.*, different weather, season or illumination [33]. The success of these multi-frame filtering methods primarily rely on leveraging temporal information—explicitly found in image sequences recorded from large outdoor real environments—for reducing high false-positive rates typically found in sequence-based place recognition tasks due to perceptual aliasing and environmental cycles [26].

However, heuristic-based sequential matching has three significant practical disadvantages. First, its computational cost scales with the dataset size, which incurs expensive memory overhead, and increases the time required to deploy on big
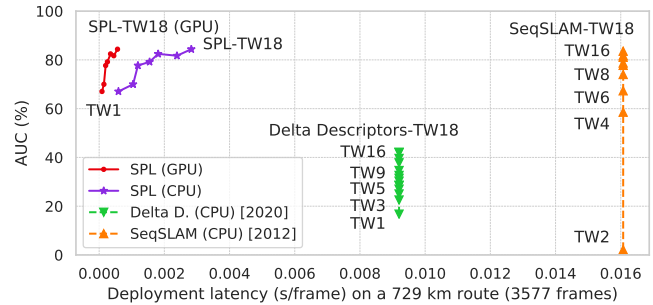
datasets or autonomous driving applications. Second, its accuracy rapidly degrades when reducing key searching parameter values such as *temporal window* (TW) lengths. Third, it typically requires both reference and query traversals during deployment, which increases storage cost with dataset size, to compute a pairwise similarity matrix that is then directly enhanced based on best-match searching heuristics or strong assumptions on velocity information for instance. Moreover, the development of entirely new multi-frame filtering methods, through the use of recurrent neural networks (RNNs) [11], suitable for learning structure in time, has been surprisingly limited; only recently the use of hand-crafted, non-trainable continuous attractor recurrent networks has been proposed [7].

In this paper, we argue that these limitations and negative consequences can be fundamentally addressed in a deep learning framework by exploiting the underinvestigated use of RNNs for sequence inference, rather than heuristic-based techniques. Hence, we build on using long short-term memory (LSTM) [19] networks for learning sequence filtering tasks, addressing all the main limitations of classical methods. Our main contributions are summarized as follows:

- We design a trainable CNN+LSTM architecture, which fuses *visual and positional* data, recorded from a single traversal of an environment, via a *sequential process*. Our approach, *Sequential Place Learning* (SPL), learns multi-frame sequential matching tasks end-to-end via backpropagation through time (BPTT) [45].
- We propose a sequence processing strategy that allows us to train our model to achieve substantially higher average-precision results using short TW lenghts, contrary to what

was known to-date based on classical sequential filtering methods for place recognition in robotics research [29].

- We present the first demonstration of high-performance learning-based sequence filtering on a range of deployment latencies (see Fig. 1), which allows us to set *new state-of-the-art results* on *4 benchmark robotic datasets*, while *outperforming 15 classical methods*.

Sequential place learning (SPL) simultaneously train two key learning-based systems: (i) a convolutional neural network (CNN) for encoding raw RGB images, and (ii) a recurrent network (LSTM) for sequential learning and inference by temporally fusing visual encodings with positional data; obtained from any source of motion estimation including but not limited to wheel/visual/radar odometry, LiDAR, GPS, structure from motion (SfM) or even synthetic time-series data.

We conduct extensive experiments to demonstrate the significance of SPL on four (4) datasets (Oxford RobotCar, Nordland Railway, St. Lucia, and Gardens Point) each recorded multiple times along 10-km, 729-km, 1-km and ∼10-km routes, respectively, with diverse conditions. On the Gardens Point dataset, in particular, we compare our model against ten (10) well-known classical methods under drastic day-night changes and show that our approach attains 100% recall rates at 100% precision for the first time.

The paper is structured as follows. We discuss the problem of multi-frame place recognition tasks while briefly surveying research papers on classical sequential filtering techniques in Section II. We introduce the concepts of *simultaneous visual-and-positional learning* and *multi-frame place learning* for route-based place recognition tasks, and describe how we developed our new state-of-the-art architectures in Section III. Finally, we present our experimental setup and results in Sections IV and V, respectively, before conclusion in Section VI; which is followed by the Appendix with additional results.

II. UNDERSTANDING SEQUENCE FILTERING

Here we first describe how pairwise (reference-query) image similarities work well for single-frame, image-retrieval-like tasks, but produce poor results when dealing with image sequences. Highlighting the need for versatile sequence filtering methods for route-based place recognition. We then briefly review prior work on sequence matching and describe the key components that might allow us to understand key strategies within classical methods in order to replicate these benefits when training neural networks for sequence modeling tasks.

A. Image Similarity

Visual place recognition research currently relies on image representations for global image description typically obtained from off-the-shelf CNN functions, rather than classical hand-crafted features such as SIFT [24] or SURF [3], pre-trained for classification [38] or image retrieval tasks [1].

B. Sequence Matching

The majority of multi-frame place recognition methods are then built based on pre-computed pairwise difference

similarity matrices, between reference and query image representations, for iteratively applying temporal filtering/searching heuristics that seek to reduce false-positive rates such as ABLE [2], ISM [42], OPR [40], VPR [41], HMM [17], MCN [33] and many others [12, 13, 33, 25, 8, 44]. The key ideas behind this, now standard, methodology date from key appearance-only topological place recognition systems such as FAB-MAP [10, 9] and SeqSLAM [30, 29].

Subsequent work that integrated odometry information was shown to improve place recognition performance such as CAT-SLAM [27] or SMART [35] on a variety of benchmark datasets [36]. The main benefits of the sequence filtering layers of these systems is that it allows robust generalization across challenging appearance and viewpoint variations including multiple seasons, weather, and lighting conditions [6]. All these models, however, share a common limitation which is that they do not incorporate modern learning-based systems, *e.g*, recurrent neural networks (RNN), for sequence inference.

III. TOWARDS SEQUENTIAL PLACE LEARNING

Only recently, researchers have shown the use of dynamical attractors neural circuits [31] (a.k.a. continuous attractor neural networks (CANN)), a neuroscience-oriented type of RNN, to perform sequential place recognition without resorting to classical methods for sequence matching [7]. This work demonstrate the potential of RNNs for temporal processing tasks in robotics research as in recent hybrid approaches [47, 43]. Although the model proposed in [7] achieves competitive results on challenging place recognition datasets, the CANN component does not incorporate learning capabilities, instead relying on pre-assigned unit interconnections and weights that need to be carefully fine-tuned to deploy on a particular dataset. Also, it does not incorporate self position-aware learning properties, rather it implements a direct mechanistic shift-and-copy action to simulate movement through the environment.

A. Joint Visual-and-Positional Place Learning

In contrast with classical two-stage multi-frame pipelines, *e.g.*, *match-then-temporally-filter*, here we propose to jointly learn visual-and-positional representations that can be simultaneously used for sequential inference for place recognition for the first time. We design and implement an entire neural network which can be trained end-to-end via BPTT [45]. In the next section, we describe how the visual and positional processing components of our architecture are integrated.

B. Neural Network Architecture

The overall CNN+LSTM architecture for *global image description* and *sequential place learning* is shown in Fig. 2(b) comprising a single CNN vision module and 2 recurrent LSTM cells, along with a baseline network (a) with an LSTM.

Global place description: Given an image sequence I_t of an environment, we apply a CNN function on each input image to obtain compact n-dimensional *global image descriptors* $\mathbf{d}_t$, where $n \in \mathbb{N}^+$ is a function of the CNN model. These representations can be learned through conventional training via
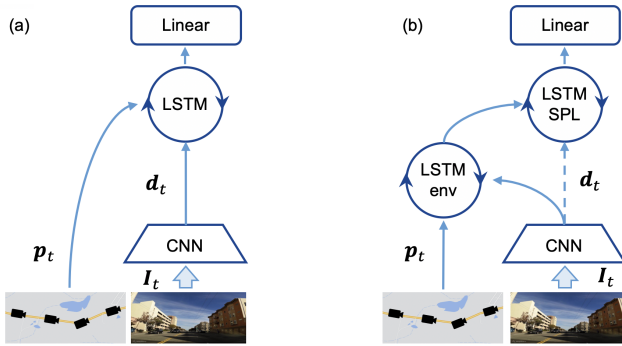
Fig. 2. (a) Baseline network. (b) Proposed CNN+LSTM architecture for positional $\mathbf{p}_t$ and visual $\mathbf{d}_t$ sequential place learning (SPL).

backpropagation. After training, the CNN will have visually encoded the entire environment within its network weights.

Sequence place learning (SPL): Depending on the type of CNN chosen, and its particular training requirements, the overall CNN+LSTM training stage can be alleviated by using a pre-trained CNN function such as NetVLAD [1], heavily used in visual place recognition research for extracting robust global image descriptors. Thus, the CCN module can be frozen while the LSTM cell are trained via BPTT [45]. In Fig. 2(b), the environment-specific (env) LSTM cell receives the CNN visual features, temporally concatenated with corresponding positional encodings. This allows our model to capture locale-specific visual and topology features that can then be used to feed a LSTM cell for SPL. The (SPL) LSTM cell receives a direct (skip) connection from the CNN module output, concatenated with the hidden states of the environment-specific LSTM output. Finally, a single linear layer (or multi-layer perceptron (MLP)) receives the hidden states from the (SPL) LSTM cell for semi-supervised training (see Fig. 2).

Implementation details: We experimented with several (pre-trained and trained from scratch) CNN vision models. Not surprisingly, we found that NetVLAD [1], a VGG-16 [37] based architecture, provided better results on average than other vanilla models including AlexNet [23], VGG-16, ResNet-18 [18], SqueezeNet [21], DenseNet-161 [20]. Thus, we used the best model (NetVLAD+whitening, trained on Pittsburgh 30k [39]), with feature dimension of $n = 4096$, from the official MATLAB implementation[1] for all state-of-the-art comparisons in Section V. The NetVLAD image descriptors $\mathbf{d}_t$ were obtained using 224×224 RGB image observations, and the 2D positional information $\mathbf{p}_t$ was encoded using a 2-d vector. Depending on the type of motion data provided by each dataset, we could use any source of motion estimation including GPS, odometry or SfM. For all experiments, we standardize $\mathbf{p}_t$ ($\mu = 0$, $\sigma = 1$) prior to feeding the network. For the recurrent networks, two vanilla single-cell LSTMs, with 512 units each, were trained end-to-end. The number of units N of the linear output layer was set to be equal to the total number of frames of the dataset minus TW length.

Learning hyperparameters: The cost function of the se-

quential inference task was sent to the Adam learning gradient algorithm [22] with plateau scheduler for reducing the learning rate (lr), with `weight_decay = 0`, `initial_lr = 0.001`, and `min_lr = 10^{-6}`. The weight assigned to the positional encodings was 500, found through cross-validation. The number of training epochs used vary depending on the dataset size. In this paper, we trained our models using 200 up to 3,000 epochs per environment, comprising between 200 and 35K+ consecutive frames, respectively, with batch sizes equal to the number of frames for stable training. After training, our models were capable of temporally integrating both vision and positional data, even using short TW lengths.

C. Sequence Processing and Temporal Window (TW)

The LSTM cell in Fig. 2 learn a function to perform sequence inference based on image and positional sequential data. To enable convergence during training, we transform these sequences of observations and states into multiple examples using a sequential processing strategy over a TW length. Given a sequence with N time steps $I_t = [I_1, I_2, ..., I_t, ..., I_N]$ (representing a sequence of raw images or positional encodings) we split this into multiple samples (sub-sequences) of TW consecutive time steps, resulting in the following N-TW samples: $S_1 = [I_1, I_2, ..., I_{TW}]$, $S_2 = [I_2, I_3, ..., I_{TW+1}]$, ... $S_{N-TW} = [I_{N-TW}, I_{N-TW+1}, ..., I_{N-1}]$. We feed our model with a `batch_size` number of these temporally synchronized, consecutive (image and positional) samples, and highlight that our implementation is robust to training and deployment with shuffled samples, and also to velocity inconsistency between training and query traversals. We provide experiments on asynchronous datasets to demonstrate this capability.

IV. EXPERIMENTAL SETUP

A. Sequence-based Datasets

Nordlandsbanen: The minute by minute, season by season Nordland Railway dataset[2] was recorded over a 729 km train journey in Norway, providing four huge ∼10-hour video streams, one for every season, at 25 FPS and 1920×1080 resolution. Each video file is synchronized in order to make the train appear to be at the same place at the same time. It also provides synchronized GPS data for each traversal. On this dataset, we conducted two main experiments by extracting individual frames out of videos at 1 FPS and 0.1 FPS, resulting in 35768 and 3577 frames, respectively. We trained our model on *summer* conditions and tested on the remaining (*fall*, *winter*, *spring*), and corresponding GPS data was encoded to represent positional information as discussed in Section III-B.

Oxford RobotCar: This dataset [28] was collected on a car platform traversing over 100+ times over a 10 km route in Oxford, UK, over a 1-year period, capturing diverse weather, season, and dynamic urban conditions. We selected 1000 temporally synchronized frames out of three traversals[3], referred here as *overcast* for training, and *sunlight* and *night*

---

[1]https://github.com/relja/netvlad

[2]https://nrkbeta.no/2013/01/15/
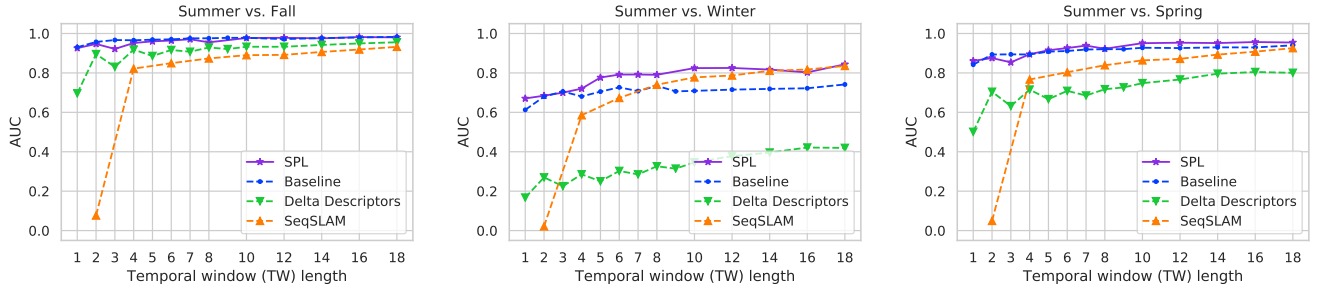[3]2014-12-09-13-21-02, 2015-05-19-14-06-38, 2014-12-10-18-10-50 in [28]

Fig. 3. **Influence of temporal window (TW)** on multi-frame methods and generalization from *summer* to *fall*, *winter* and *spring* conditions of Nordland.
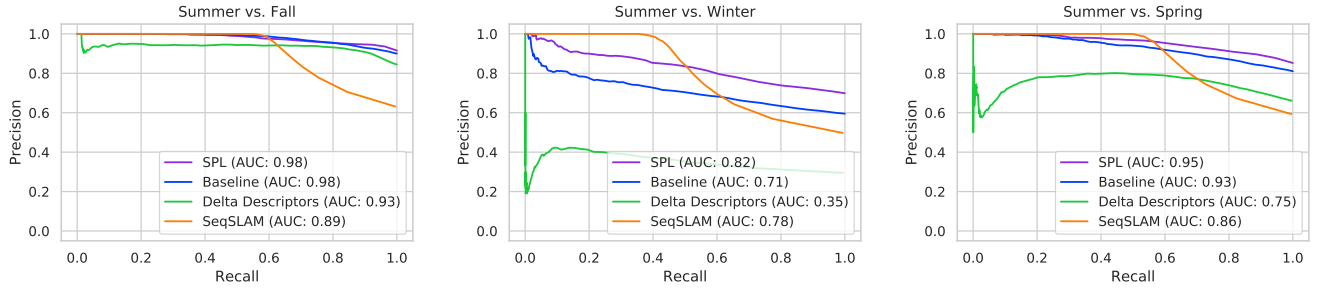

Fig. 4. **Precision-recall curves and AUC metrics on the Nordland dataset** using a localization radius of 10 frames and TW of 10.

for testing, with corresponding GPS data. On this particular dataset, we used 1280×960 RGB images from the center side of the Bumblebee XB3 trinocular camera but without applying undistortion, thus, slightly increasing the difficulty for recognizing places.

Gardens Point: The day and night with lateral pose change (right, left) Gardens Point Walking dataset [14] consists of three synchronized traversals with 200 images at 960×540 resolution each. We conduct several experiments for viewpoint and appearance changes on this dataset by training and testing on different traversal combinations as detailed in Section V. This dataset does not provide motion information but we use synthetic time-series data provided in [6].

St Lucia: The St Lucia Multiple Times of Day dataset [15] was collected with a forward facing webcam, attached to the roof of a car, through the suburb of St Lucia, Queensland, Australia. The route was traversed ten times during multiple days to capture the difference in appearance between early morning and late afternoon. GPS data is included for each trip and synchronized with 640×480 RBG images at 15 FPS. On this dataset, we demonstrate that our approach is robust to strong velocity inconsistencies of the car between training and query traversals. We use the first 4,000 frames of each traversal, covering the full ∼10-km perimeter of the suburb.

B. Precision-Recall, Average-Precision and Tolerances

Precision-Recall and Average-Precision: On deployment, likelihood scores for each query image w.r.t. the reference traversal are produced by the linear output layer of our model. These values were then used to compute corresponding precision-recall (PR) curves, which can then be used to

calculate other types of metrics such as area under the curve (AUC). We report both PR curves and AUC metrics for all experiments and datasets.

Coarse Localization Radius Tolerance: Except for St Lucia, we report results on a range of ground-truth error tolerance from 1 up to 50 frames away from the correct match for performance analysis in Section V. On St Lucia, we consider a localization radius tolerance of 20 meters.

V. RESULTS

Here we demonstrate that our approach is capable of learning sequence inference from a single traversal of a route, while accurately generalizing to multiple traversals of that route under very different visual conditions. Also, on the most challenging asynchronous dataset, St Lucia, with velocity inconsistencies, our approach gets 96.65% AUC while SeqSLAM and Delta Descriptors struggle with 27.39% AUC and 57.47% AUC, respectively.

A. Influence of Temporal Window (TW)

In Fig. 3 we demonstrate how classical methods such as SeqSLAM [30] and Delta Descriptors [13] struggle to produce accurate results when using short TW lengths, especially under strong visual changes as discussed throughout the paper, while learning-based methods achieve competent AUC results above 60%. We used a localization radius tolerance of 10 frames for producing this figure at every single value of TW, which is lower than in previous research [6]. For SeqSLAM, we use the official MATLAB implementation[4] with default parameters

---

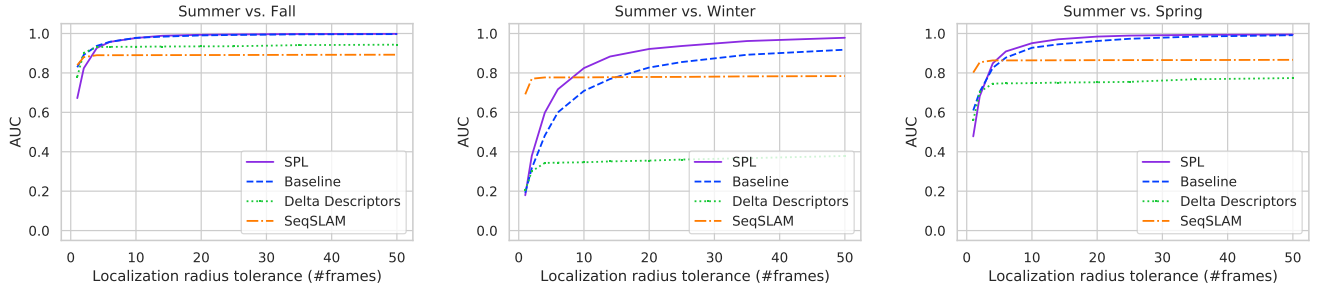[4]https://github.com/OpenSLAM-org/openslam_openseqslam

Fig. 5. **AUC metrics vs. localization radius tolerance on the Nordland dataset** with TW of 10.

TABLE I
SPACE AND TIME SYNCHRONIZED DATASETS: AUC (%) RESULTS FOR LOCALIZATION RADIUS OF 2/10/50 AND TW OF 10

Method	Gardens Point		Nordlandsbanen		Oxford RobotCar	
	Day (L)-Night (R)	Day (R)-Day (L)	Summer-Fall	Summer-Winter	Overcast-Sunlight	Overcast-Night
SeqSLAM [30]	5.2 / 12.8 / 46.2	43.2 / 56.5 / 65.8	88.0 / 89.0 / 89.2	**77.0** / 77.7 / 78.3	9.4 / 16.9 / 18.6	1.3 / 3.9 / 12.0
Delta D. (DD) [13]	79.8 / 93.8 / 96.6	96.1 / 99.5 / 99.5	**90.2** / 93.2 / 94.3	30.0 / 34.6 / 37.8	4.9 / 16.1 / 27.2	**87.1** / 87.1 / 87.1
Baseline (BL) [6]	**100 / 100 / 100**	**100 / 100 / 100**	89.1 / **97.8** / 99.6	31.6 / 70.9 / 91.7	**78.4** / 96.7 / **100**	69.6 / 93.1 / 99.3
SPL	**100 / 100 / 100**	**100 / 100 / 100**	82.3 / **97.8** / **99.8**	37.8 / **82.4** / **97.8**	66.9 / **97.9** / **100**	53.2 / **96.0** / **99.9**

TABLE II
ASYNCHRONOUS DATASETS: AUC (%) RESULTS FOR LOCALIZATION RADIUS OF 20 METERS AND TW OF 10

Method	St Lucia							
	100909_1000	100909_1210	100909_1410	110909_1545	180809_1545	190809_1410	210809_1000	210809_1210
SeqSLAM [30]	61.64	50.04	48.74	27.39	44.12	61.32	44.51	38.19
DD [13]	97.89	92.71	78.03	57.47	74.58	67.28	98.98	92.79
SPL	**99.94**	**99.68**	**99.54**	**96.65**	**98.99**	**99.61**	**99.78**	**97.07**

(only changing TW or d_s as needed); SeqSLAM only works using an even number for d_s though. For Delta Descriptors, we use the Python code provided by the authors in [13] with default parameters also varying TW only as needed. We highlight that the baseline [6], is getting competitive performance with its generalized method but under *summer-winter* changes its performance remains constant at 70% AUC, even using larger TWs, while our approach and SeqSLAM achieve over 80% AUC. However, when using a TW of 2 frames (Fig. 3-Middle), SeqSLAM and Delta Descriptors get 2% and 27% AUC, respectively, while ours gets near 70%.

B. Comparisons on Space and Time Synchronized Datasets

In Fig. 4 we report the PR curves for a TW of 10 obtained from the results on Fig. 3, with corresponding AUC metrics, considering a localization radius tolerance of 10 frames. On the most challenging *summer-winter* conditions changes, we note that SeqSLAM performs competitively at this TW with 78% AUC on *winter* (Fig. 4-middle), but our model outperforms it with 82% AUC overall. At the same conditions, Delta Descriptors is shown to perform poorly due to both image resolution and huge sampling rates sensitivity on this particular dataset settings. We will show, however, that its performance gets better on the other dataset configurations for fair comparisons, but we wanted to highlight this particular limitation among classical methods. Nevertheless, on the other

less challenging conditions changes (*fall*, *spring*), we show all these models achieve competent results approaches 75%.

More generally, in Fig. 5, we show how the AUC spectrum changes against localization radius tolerances between 1 to 50 frames, while all models are using a standard value of TW=10; typically used on place recognition research. We also highlight that TW of 10 effectively captures the overall maximum AUC results of each method, as shown in Fig. 3. In Table I we summarize the main AUC results corresponding to our three datasets for a TW of 10 and localization radius of 2/10/50 frames. Our model consistently attains higher AUC values than classical methods at challenging visual transitions such as *day-night* and *summer-winter*. In the Appendix we report all the PR curves from where the AUC metrics presented in Table I were obtained, along with the training curves of our approach.

C. Comparisons on Asynchronous Datasets

In Table II, we report the results on the St Lucia dataset, recorded under variable velocities of the vehicle as discussed in Sections IV and III-C. We show AUC values for late morning and all afternoon times (totaling 8 query traversals), given that our reference traversal was recorded early morning around 08:45 a.m. (190809_0845). In the Appendix, however, we show the full PR curves and qualitative results on the full 10 subsets for each method. Our approach again significantly outperforms other methods on all the subsets.

Traversal		Methods with NetVLAD Front-End										
Ref	Query	Pairwise	ABLE [2]	ISM [42]	OPR [40]	VPR [41]	HMM [17]	SeqSLAM	MCN [33]	DD	BL	SPL
D-L	N-R	0.41	0.79	0.61	0.48	0.29	0.02	0.15	0.43	0.93	0.99	1
D-R	D-L	0.98	1	0.69	0.69	0.69	0.33	0.68	0.99	0.99	0.99	1
D-R	N-R	0.52	0.8	0.64	0.64	0.47	0.20	0.30	0.54	0.98	0.99	1

Changes	Viewpoint		Appearance		Viewpoint & Appearance	
Dataset	Gardens Point	CSU-1	Gardens Point	Nordland	Gardens Point	CSU-2
Reference-Query	Day (L)-Day (R)	Day (L)-Day (R)	Day (R)-Night (R)	Summer-Winter	Day (L)-Night (R)	Day (L)-Day (R)
FAB-MAP [10]	2.0	14.3	-	-	-	-
VLAD-based [25]	19.5	59.0	2.5	2.0	-	11.0
SeqSLAM [30]	1.0	25.9	3.0	4.6	-	16.0
SMART [35]	13.0	12.5	5.0	4.4	-	1.0
CNN+Seq [8]	45.0	67.9	48.0	9.0	14.0	41.0
RISF [44]	46.0	91.0	63.0	22.9	67.5	90.0
Baseline [6]	99.0	100	99.0	1.2	99.0	100
SPL	100	100	100	2.5	100	100

D. Comparison to Ten Methods using the Same Front-End

All the results reported in Section V-B were obtained using their original fron-end methods for global image description. SeqSLAM used classical sum of absolute differences (SAD), and the others (Delta Descriptors, Baseline, and our approach) by default use the best NetVLAD model as we described in Section III-B. In Table III, we report additional supporting comparisons against single-frame vanilla NetVLAD (pairwise) and other 6 multi-frame filtering methods (ABLE [2], ISM [42], OPR [40], VPR [41], HMM [17], SeqSLAM [30], MCN [33]) that received the pairwise similarity matrix, obtained from NetVLAD [1], for sequence filtering according to [33]. In addition to SeqSLAM, Delta Descriptors (DD) and Baseline (BL), in Table III we present the full comparison all these ten methods on the Gardens Point dataset. AUC results are calculated with the same localization tolerance used in [33]. Our model outperforms all the others with 100% recall at 100% precision on all the required reference-query combinations of subsets: day-left (D-L), day-right (D-R) and night-right (N-R).

E. Robustness to Viewpoint and Appearance Changes

In Table IV, we reproduce the benchmark presented in [44] where the authors compare their model under changes in viewpoint, appearance and both types of changes at the same time on three datasets. This allows us to compare our approach against five other methods such as FAB-MAP [10], VLAD-based [25], SMART [35], CNN+Seq [8], Robust Image-sequence-based framework (RISF) [44], in addition to SeqSLAM and the baseline network. Our best model once again achieves precision rates of 100% at 100% recall on all but one condition. Where the method in [44] performs the best with 22.9% recall, while ours gets 2.5% recall. It is worth noting, however, that our model can achieve up to 82% AUC on this particular condition, which on average is comparable to ∼ 88% AUC of the method proposed in [44] according to their

Method	35,768 frames	3,577 frames
SeqSLAM (CPU)	70m	57s
Delta Descriptors (CPU)	51m	33s
SPL (CPU)	1m	5.7s

PR curves. Overall at this point we have already compared SPL against 15 place recognition systems on 5 datasets.

F. High-Performance Analysis

In Table V we compare the runtime on deployment using the same CPU (Intel Core i7-8700K CPU @3.70GHz) for all these models on our two (large and medium) Nordland dataset settings, comprising 35,768 and 3,577 frames, respectively. For a medium dataset size, our CPU-based model is up to 10× faster than classical methods, while for the large dataset configuration it can be up to 70× faster. It is worth noting that these speed-ups are based on the average latency of our model running on CPU only (not on GPU). Our model SPL running on a GPU (GeForce GTX 1080Ti), shown in red in Fig. 1, is even faster but we do not compare the latency of classical methods against our GPU deployment. In Fig. 1, we show the performance comparison between AUC metrics and deployment latency for our medium dataset configuration, where we vary TW from 1 up to 18. All our models achieve comparable results to the best SeqSLAM settings (with TW of 18), even with TW values around 5. Although we used CPU for comparison purposes, we highlight that the PyTorch [34] implementation can run on CPU or GPU, contrary to classical methods that typically run on CPU.

G. Qualitative Results

In Figs. 6, 7 and 8, we show visualizations of the raw sequence-based image matchings on the Gardens Point, Nord-

Fig. 6. Deployment on Gardens Point with TW and tolerance of 10.

Fig. 7. Deployment on Nordlandsbanen with TW and tolerance of 10.

land and Oxford RobotCar datasets, respectively, along the entire traversal we used for each experiment. From left to right, in each figure, every column shows the top-1 match for a particular reference image (left), obtained using our approach (SPL), SeqSLAM and Delta Descriptors (right). The reference sequence was obtained by sampling 10 equally-spaced images out of the entire traversal, each traversal starting on the top and ending on the bottom of the figure. In the Appendix, we show similar qualitative results on the St Lucia dataset, but for the full 10 traversals and considering 20 equally-spaced images sampled from the entire reference traversal.

VI. DISCUSSION AND CONCLUSIONS

We designed and implemented an LSTM-based architecture for joint visual-and-positional encoding and sequential place learning (SPL), rather than using conventional two-stage *match-then-filter* techniques. SPL was shown to be robust to extreme environmental changes and velocity inconsistency between training and query traversals, found across four large, challenging benchmark driving datasets. Our approach addressed all the main limitations of classical heuristic-based methods including high sensitivity to short temporal windows (TW) values, expensive compute and storage requirements and

very limited work on learning-based systems for sequence inference using recurrent networks. It provides a strong baseline for future work in learning-based sequence filtering in the context of simultaneous localization and mapping (SLAM) and autonomous navigation research.

We proposed a generalized CNN+LSTM model that incorporates an *environment-specific* LSTM cell for potentially enabling learning across different environments. This apparently simple yet more general architectural change, compared to a baseline that uses a single-cell LSTM, was found to be even more accurate and robust, while also potentially enabling further extension of our approach onto a *multi-environment architecture* for training and deployment on different environments using a single model; as in related reinforcement-learning-based research for navigation [32].

Instead of relying on pre-trained CNN models, we set out to use a small two-layer CNN for exploring the end-to-end training behavior (from scratch) of our model but the results showed that the CNN component does not generalize well to drastic visual changes, which was expected since these models require a significant amount of data for effective training and generalization. We see this observation as future work to further investigate additional advantages of jointly learning visual

| Reference | SPL | SeqSLAM | Delta Descriptors |

Fig. 8. Deployment on Oxford RobotCar with TW and tolerance of 10.

and positional information. Finally, it is worth noting that our method has the potential for supporting the development of a full learning-based SLAM system by incorporating a geometric mapping neural network such as those in [5, 4, 46].

REFERENCES

[1] Relja Arandjelović, Petr Gronát, Akihiko Torii, Tomás Pajdla, and Josef Sivic. NetVLAD: CNN Architecture for Weakly Supervised Place Recognition. *2016 IEEE Conference on Computer Vision and Pattern Recognition (CVPR)*, pages 5297–5307, 2016.

[2] Roberto Arroyo, Pablo F Alcantarilla, Luis M Bergasa, and Eduardo Romera. Towards life-long visual localization using an efficient matching of binary sequences from images. In *2015 IEEE international conference on robotics and automation (ICRA)*, pages 6328–6335. IEEE, 2015.

[3] Herbert Bay, Tinne Tuytelaars, and Luc Van Gool. Surf: Speeded up robust features. In *European conference on computer vision*, pages 404–417. Springer, 2006.

[4] Jia-Wang Bian, Zhichao Li, Naiyan Wang, Huangying Zhan, Chunhua Shen, Ming-Ming Cheng, and Ian Reid. Unsupervised scale-consistent depth and ego-motion learning from monocular video. In *NeurIPS*, 2019.

[5] Samarth Brahmbhatt, Jinwei Gu, Kihwan Kim, James Hays, and Jan Kautz. Geometry-aware learning of maps for camera localization. In *IEEE Conference on Computer Vision and Pattern Recognition (CVPR)*, 2018.

[6] Marvin Chancán and Milford Milford. DeepSeqSLAM: A Trainable CNN+RNN for Joint Global Description and Sequence-based Place Recognition. *arXiv preprint arXiv:2011.08518*, 2020.

[7] Marvin Chancán, Luis Hernandez-Nunez, Ajay Narendra, Andrew B. Barron, and Michael Milford. A hybrid compact neural architecture for visual place recognition. *IEEE Robotics and Automation Letters*, 5(2):993–1000, April 2020. ISSN 2377-3774. doi: 10.1109/LRA.2020. 2967324.

[8] Zetao Chen, Obadiah Lam, Adam Jacobson, and Michael Milford. Convolutional neural network-based place recognition. *arXiv preprint arXiv:1411.1509*, 2014.

[9] Mark Cummins. Highly scalable appearance-only slam-fab-map 2.0. *Proc. Robotics: Sciences and Systems (RSS), 2009*, 2009.

[10] Mark Cummins and Paul Newman. Fab-map: Probabilistic localization and mapping in the space of appearance. *The International Journal of Robotics Research*, 27(6): 647–665, 2008.

[11] Jeffrey L. Elman. Finding structure in time. *Cognitive Science*, 14(2):179–211, 1990. doi: https://doi.org/10. 1207/s15516709cog1402_1.

[12] Matthew Gadd, Daniele De Martini, and Paul Newman. Look around you: Sequence-based radar place recognition with learned rotational invariance. In *2020 IEEE/ION Position, Location and Navigation Symposium (PLANS)*, pages 270–276, 2020.

[13] Sourav Garg, Ben Harwood, Gaurangi Anand, and Michael Milford. Delta descriptors: Change-based place representation for robust visual localization. *IEEE Robotics and Automation Letters*, 5(4):5120–5127, 2020.

[14] Arren Glover. Day and night with lateral pose change datasets. 2014. doi: http://doi.org/10.5281/zenodo. 4561862.

[15] Arren Glover, Will Maddern, Michael Milford, and Gordon Wyeth. FAB-MAP+RatSLAM: Appearance-based SLAM for Multiple Times of Day. In *ICRA*, Anchorage, USA, 2010.

[16] Ian G Goodfellow, Yoshua Bengio, and Aaron C. Courville. Deep learning. *Nature*, 521:436–444, 2015.

[17] Peter Hansen and Brett Browning. Visual place recognition using hmm sequence matching. In *2014 IEEE/RSJ International Conference on Intelligent Robots and Systems*, pages 4549–4555. IEEE, 2014.

[18] Kaiming He, Xiangyu Zhang, Shaoqing Ren, and Jian Sun. Deep residual learning for image recognition. In *Proceedings of the IEEE conference on computer vision and pattern recognition*, pages 770–778, 2016.

[19] Sepp Hochreiter and Jürgen Schmidhuber. Long short-

term memory. *Neural Computation*, 9:1735–1780, 1997.

[20] Gao Huang, Zhuang Liu, Laurens van der Maaten, and Kilian Q. Weinberger. Densely connected convolutional networks. In *Proceedings of the IEEE Conference on Computer Vision and Pattern Recognition (CVPR)*, 2017.

[21] Forrest N Iandola, Song Han, Matthew W Moskewicz, Khalid Ashraf, William J Dally, and Kurt Keutzer. Squeezenet: Alexnet-level accuracy with 50x fewer parameters and <0.5 mb model size. *arXiv preprint arXiv:1602.07360*, 2016.

[22] Diederik P. Kingma and Jimmy Ba. Adam: A method for stochastic optimization. *arXiv preprint arXiv:1412.6980*, 2014.

[23] Alex Krizhevsky. One weird trick for parallelizing convolutional neural networks. *arXiv preprint arXiv:1404.5997*, 2014.

[24] David G Lowe. Object recognition from local scale-invariant features. In *Proceedings of the seventh IEEE international conference on computer vision*, volume 2, pages 1150–1157. Ieee, 1999.

[25] Stephanie Lowry and Henrik Andreasson. Lightweight, viewpoint-invariant visual place recognition in changing environments. *IEEE Robotics and Automation Letters*, 3 (2):957–964, 2018.

[26] Stephanie Lowry, Niko Sünderhauf, Paul Newman, John J Leonard, David Cox, Peter Corke, and Michael J Milford. Visual place recognition: A survey. *IEEE Transactions on Robotics*, 32(1):1–19, Feb 2016.

[27] Will Maddern, Michael Milford, and Gordon Wyeth. Cat-slam: probabilistic localisation and mapping using a continuous appearance-based trajectory. *The International Journal of Robotics Research*, 31(4):429–451, 2012.

[28] Will Maddern, Geoffrey Pascoe, Chris Linegar, and Paul Newman. 1 year, 1000 km: The oxford robotcar dataset. *The International Journal of Robotics Research*, 36(1): 3–15, 2017.

[29] Michael Milford. Vision-based place recognition: how low can you go? *The International Journal of Robotics Research*, 32(7):766–789, 2013.

[30] Michael J Milford and Gordon F Wyeth. SeqSLAM: Visual route-based navigation for sunny summer days and stormy winter nights. In *2012 IEEE International Conference on Robotics and Automation (ICRA)*, pages 1643–1649, May 2012.

[31] Paul Miller. Dynamical systems, attractors, and neural circuits. *F1000Research*, 5(F1000 Faculty Rev):992, 2016. doi: https://doi.org/10.12688/f1000research.7698.1.

[32] Piotr Mirowski *et al.* Learning to navigate in cities without a map. In *NIPS*, pages 2419–2430, 2018.

[33] Peer Neubert, Stefan Schubert, and Peter Protzel. A neurologically inspired sequence processing model for mobile robot place recognition. *IEEE Robotics and Automation Letters*, 4(4):3200–3207, 2019.

[34] Adam Paszke et al. Pytorch: An imperative style, high-performance deep learning library. In *NeurIPS*, pages 8026–8037. 2019.

[35] Edward Pepperell, Peter I Corke, and Michael J Milford. All-environment visual place recognition with smart. In *IEEE International Conference on Robotics and Automation (ICRA)*, pages 1612–1618, 2014.

[36] Stefan Schubert, Peer Neubert, and Peter Protzel. Towards combining a neocortex model with entorhinal grid cells for mobile robot localization. In *2019 European Conference on Mobile Robots (ECMR)*, pages 1–8. IEEE, 2019.

[37] Karen Simonyan and Andrew Zisserman. Very deep convolutional networks for large-scale image recognition. *arXiv preprint arXiv:1409.1556*, 2014.

[38] Niko Sünderhauf, Sareh Shirazi, Adam Jacobson, Feras Dayoub, Edward Pepperell, Ben Upcroft, and Michael Milford. Place recognition with convnet landmarks: Viewpoint-robust, condition-robust, training-free. *Proceedings of Robotics: Science and Systems XII*, 2015.

[39] Akihiko Torii, Josef Sivic, Tomas Pajdla, and Masatoshi Okutomi. Visual place recognition with repetitive structures. *IEEE Transactions on Pattern Analysis and Machine Intelligence*, 37(11):2346–2359, 2015.

[40] Olga Vysotska and Cyrill Stachniss. Lazy data association for image sequences matching under substantial appearance changes. *IEEE Robotics and Automation Letters*, 1(1):213–220, 2015.

[41] Olga Vysotska and Cyrill Stachniss. Relocalization under substantial appearance changes using hashing. In *Proceedings of the IROS Workshop on Planning, Perception and Navigation for Intelligent Vehicles, Vancouver, BC, Canada*, volume 24, 2017.

[42] Olga Vysotska, Tayyab Naseer, Luciano Spinello, Wolfram Burgard, and Cyrill Stachniss. Efficient and effective matching of image sequences under substantial appearance changes exploiting gps priors. In *2015 IEEE International Conference on Robotics and Automation (ICRA)*, pages 2774–2779. IEEE, 2015.

[43] Guanrui Wang, Songchen Ma, Yujie Wu, Jing Pei, Rong Zhao, and Luping Shi. End-to-end implementation of various hybrid neural networks on a cross-paradigm neuromorphic chip. *Frontiers in Neuroscience*, 15, 2021.

[44] Y. Wang, T. Xue, and Q. Li. A robust image-sequence-based framework for visual place recognition in changing environments. *IEEE Transactions on Cybernetics*, pages 1–12, 2020. doi: 10.1109/TCYB.2020.2977128.

[45] Paul J. Werbos. Generalization of backpropagation with application to a recurrent gas market model. *Neural Networks*, 1(4):339–356, 1988.

[46] Wang Zhao, Shaohui Liu, Yezhi Shu, and Yong-Jin Liu. Towards better generalization: Joint depth-pose learning without posenet. In *Proceedings of IEEE Conference on Computer Vision and Pattern Recognition (CVPR)*, 2020.

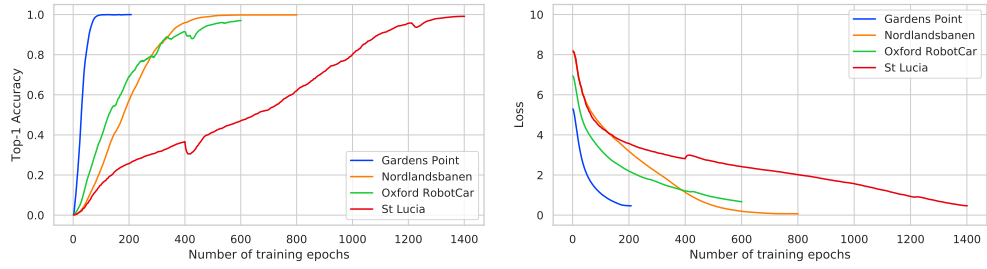[47] Zhe Zou et al. A hybrid and scalable brain-inspired robotic platform. *Scientific reports*, 10(1):1–13, 2020.

VII. Appendix

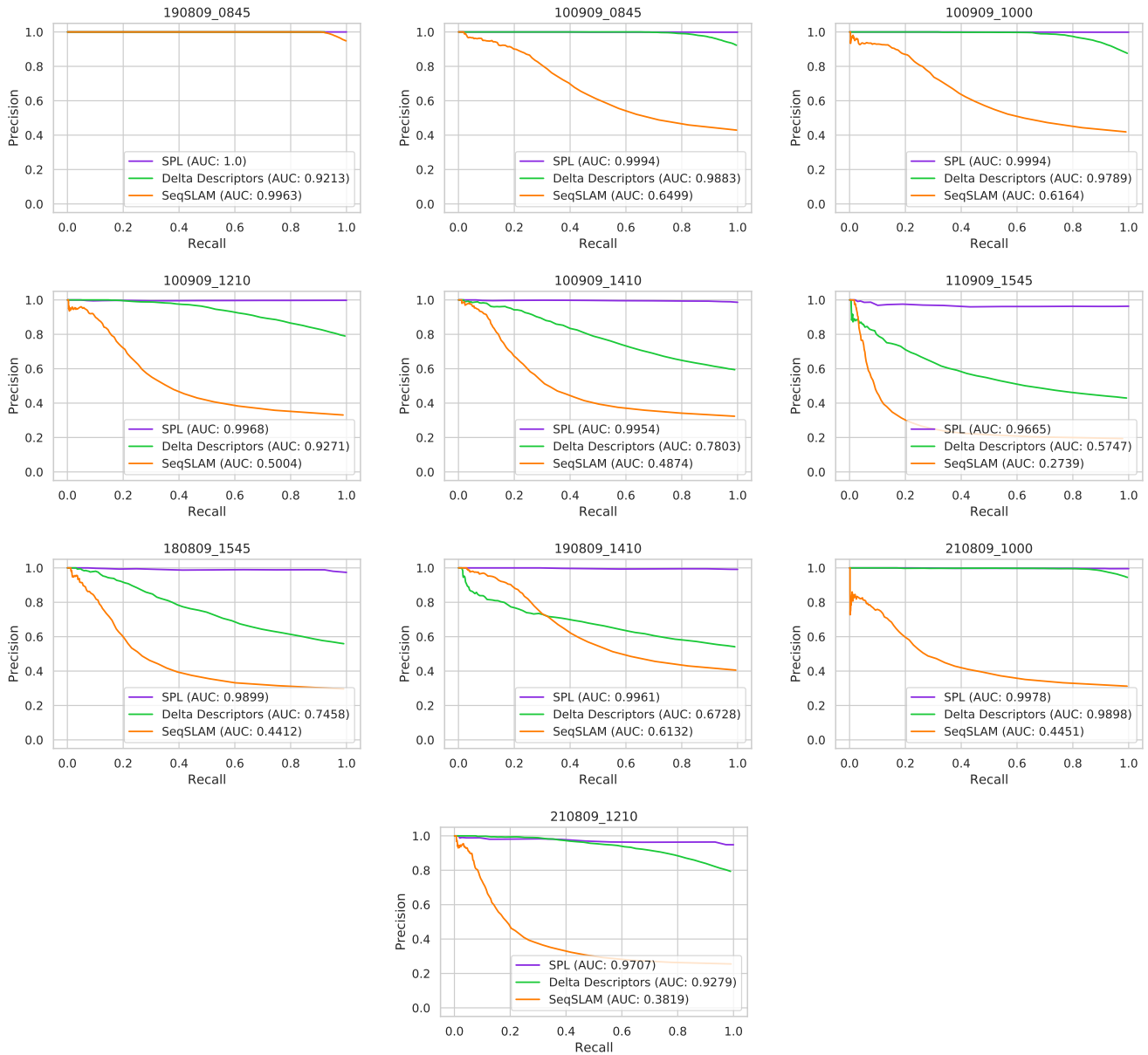Fig. 9. Top-1 accuracy and loss cost vs. training epochs.

Fig. 10. **PR curves using a tolerance of 20 meters at a sequence length of 10** on St Lucia. Reference traversal: 190809_0845.
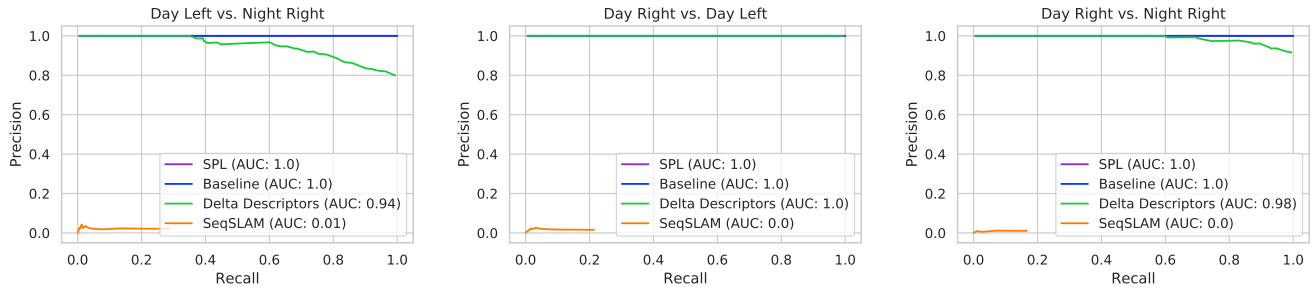
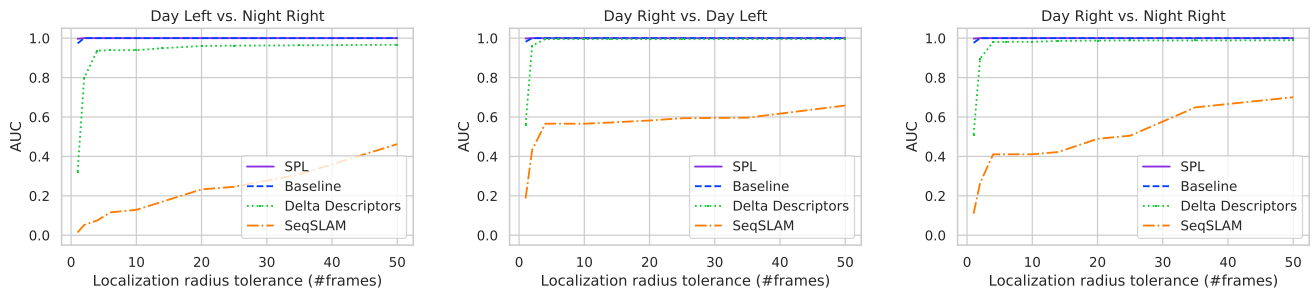Fig. 11. **PR curves using a tolerance of 10 at a sequence length of 10** on Gardens Point.

Fig. 12. **AUC vs. localization tolerance at a sequence length of 10** on Gardens Points.
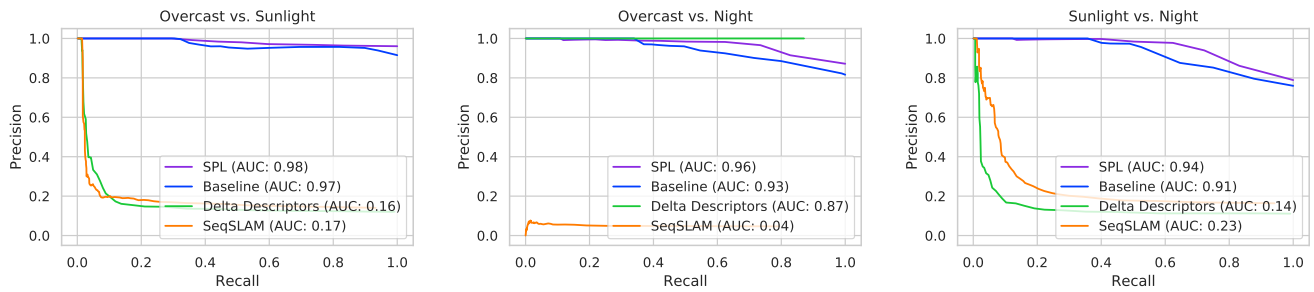

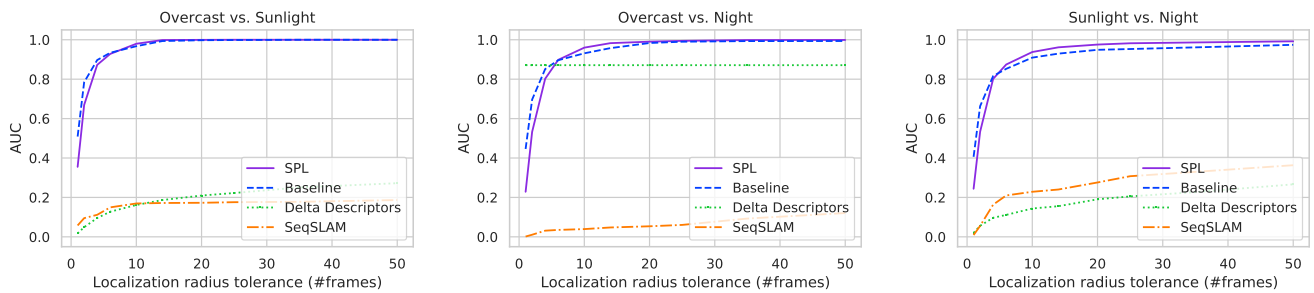Fig. 13. **PR curves using a tolerance of 10 at a sequence length of 10** on Oxford RobotCar.

Fig. 14. **AUC vs. localization tolerance at a sequence length of 10** on Oxford RobotCar.

Reference 190809_0845 100909_0845 100909_1000 100909_1210 100909_1410 110909_1545 180809_1545 190809_1410 210809_1000 210809_1210

Fig. 15. SPL deployment on St. Lucia. Reference traversal: 190809_0845.

Reference 190809_0845 100909_0845 100909_1000 100909_1210 100909_1410 110909_1545 180809_1545 190809_1410 210809_1000 210809_1210

Fig. 16.   Delta Descriptors deployment on St Lucia. Reference traversal: 190809_0845.

Reference   190809_0845 100909_0845 100909_1000 100909_1210 100909_1410 110909_1545 180809_1545 190809_1410 210809_1000 210809_1210

Fig. 17.   SeqSLAM deployment on St Lucia. Reference traversal: 190809_0845.